Journal of Advanced Ceramics
2015, **4**(4): 282–291
DOI: 10.1007/s40145-015-0162-0

ISSN 2226-4108
CN 10-1154/TQ

Research Article

Investigation of the phase space in lead-free $(K_xNa_{1-x})_{1-y}Li_y(Nb_{1-z}Ta_z)O_3$ ferroelectric ceramics

Henry E. MGBEMERE[a,b,*], Rolf JANSSEN[b], Gerold A. SCHNEIDER[b]

[a]*Department of Metallurgical & Materials Engineering, University of Lagos, Akoka, Lagos, Nigeria*
[b]*Institute of Advanced Ceramics, Hamburg University of Technology, Denickestrasse 15, 21073 Hamburg, Germany*

Received: April 15, 2015; Revised: July 10, 2015; Accepted: July 14, 2015

Abstract: A library of ceramic compounds based on the lead-free $(K_xNa_{1-x})_{1-y}Li_y(Nb_{1-z}Ta_z)O_3$ solid solution has been synthesized and characterized using high-throughput experimentation (HTE) method. The phase space previously reported by Saito and Takao has been expanded to {{x, 0.1, 1.0}, {y, 0, 0.1}, {z, 0, 0.2}}, and new phase boundaries are observed. The relative density values show that with the appropriate sintering temperature, ~92% of the theoretical density can be reached. The relative permittivity values show that with increasing amount of K^+ and Ta^{5+}, the dielectric constant values increase. The effect of density on the dielectric constant values is however minimal. Resistivity values ranging from 10^9 to 10^{13} Ω·cm are obtained for the samples. The piezoelectric charge coefficient values for selected compositions show that higher values are obtained close to the phase boundaries rather than away from them. The properties for the ceramic library using the HTE method are generally 15%–20% less than from the conventional method. This method is therefore more suited for screening of sample compositions than for producing samples with high piezoelectric properties.

Keywords: ferroelectrics; high-throughput synthesis; $(K_xNa_{1-x})NbO_3$ (KNN); lead-free ceramics

1 Introduction

The toxic nature of lead-based piezoelectric ceramics and legislations restricting their use have made it necessary for alternative compositions which are more environmentally friendly to be researched on for being possibly used as replacement materials [1]. $(K_xNa_{1-x})NbO_3$ (KNN) [2–4] and $(Bi_{0.5}Na_{0.5})TiO_3$ [5,6] based piezoelectric ceramics are currently the most likely alternatives to replace the lead-based ceramics because of their promising properties. High-throughput experimentation (HTE) is the use of miniaturization, robotics, and parallel techniques to increase research productivity, while the screening and/or analysis involve using a parallel assay to rapidly assess the properties of the samples produced [7]. The need to discover new material compositions with better properties while also limiting the amount of raw materials and time required is the driving force for this process [8]. This method has been used for thin film ceramic processing where there is need for flexibility in the change of composition [9,10]. For bulk ceramic synthesis where mixing, conditioning, shaping, and heat treatment are required before a finished product can be obtained, it proves to be more difficult using this method. The HTE method has been used in this work to produce a ceramic library with as many compositions as possible in the shortest possible time

* Corresponding author.
E-mail: henrymgbemere@yahoo.com, hmgbemere@unilag.edu.ng

[11,12]. Saito and Takao [13] reported the properties of $(K_xNa_{1-x})_{1-y}Li_y(Nb_{1-z}Ta_z)O_3$ solid solution which have much higher piezoelectric properties compared to the undoped $(K_xNa_{1-x})NbO_3$ ceramics. The improvement in piezoelectric properties was attributed to the occurrence of the so-called morphotropic phase boundary (MPB) in the system. It has been discovered that the piezoelectric properties of doped KNN ceramics are strongly dependent on the temperature leading to this phenomenon being revised to a polymorphic phase boundary (PPB), since the enhancement in piezoelectric properties is strongly related to the decrease in the phase transition temperatures [14]. There are a lot of reports in the literature about $(K_xNa_{1-x})_{1-y}Li_y(Nb_{1-z}Ta_z)O_3$ ceramics where different parameters were investigated [15–18]. In most of these reports, the composition of interest is mainly at equal amounts of the A- and B-site elements. Following the reports by Saito and Takao [13], the phase space of $(K_xNa_{1-x})_{1-y}Li_y(Nb_{1-z}Ta_z)O_3$ solid solution has been expanded in the following format {{x, 0.1, 1.0}, {y, 0, 0.1}, {z, 0, 0.2}}. The objective of this work is to use the high-throughput experimentation method in expanding the phase space in order to search for new phase boundaries with possibly better piezoelectric charge coefficient values compared to what has been reported in the literature.

2 Experimental procedure

The starting materials used for the synthesis consisted of raw powders of K_2CO_3, Na_2CO_3, Li_2CO_3 (99%), Nb_2O_5, and Ta_2O_5 (99.9%) (Chempur Feinchemikalien und Forschungs GmbH Karlsruhe, Germany). The powders were dried in an oven at 200 ℃ to remove any possible moisture present, and then 1100 mg of powders were weighed in the following format {{x, 0.1, 1.0}, {y, 0, 0.1}, {z, 0, 0.2}} using a dosing robot (Chemspeed Technologies AG Augst, Switzerland). The schematic representation of the investigated phase space in the $(K_xNa_{1-x})_{1-y}Li_y(Nb_{1-z}Ta_z)O_3$ solid solution is shown in Fig. 1. In the powder formulations, an excess of 2 mol% of Na_2CO_3 and K_2CO_3 was added to compensate for the volatile nature during sintering. Each of the dosed powders was mixed using a speed mixer (DAC-150 FVZ Hauschild Engineering, Germany) operating at 1600 rpm for 1 min. A planetary ball mill which has been modified to mill 16 different powder compositions at the same time was used for the milling. It was carried out at 200 rpm for 3 h using ethanol as solvent and ZrO_2 balls of 1 mm diameter as grinding media. The particle sizes of the powders were measured using a laser scattering size distribution analyzer (Mastersizer 2000E, Malvern Instruments Worcestershire, UK). The suspension was vacuum dried, and the calcination was done in a tube furnace at 750 ℃ for 4 h. The milling process was repeated to reduce the average powder particle size to below 1 μm. The dried powders were put in a silicone mould and pressed into tablets of ~7.5 mm in diameter and 2.0 mm in thickness using a cold isostatic press operating at 300 MPa for 2 min. Sintering was done in a chamber furnace at temperatures ranging from 1050 to 1150 ℃ for 1 h depending on the composition of the sample. Due to the nature of the experiment, two samples were produced for each composition and the density measurements were made on these samples.

The higher the Ta content of the sample, the higher the required sintering temperature. The bulk densities of the sintered samples were determined at room temperature using Archimedes method. The theoretical density for each composition was estimated based on assumptions of the expected composition and a tetragonal crystal structure at room temperature. The samples were ground and polished in preparation for characterization. The phases present in the samples were examined in an automated mode using X-ray diffraction (XRD; D8 Discover, Bruker AXS, Karlsruhe, Germany) with Cu Kα radiation (λ = 1.54056 Å), Göbel mirror, and general analysis diffraction detection system (GADDS). Six independent XRD patterns were recorded on selected positions on the surface of the sample from 20° to 60°

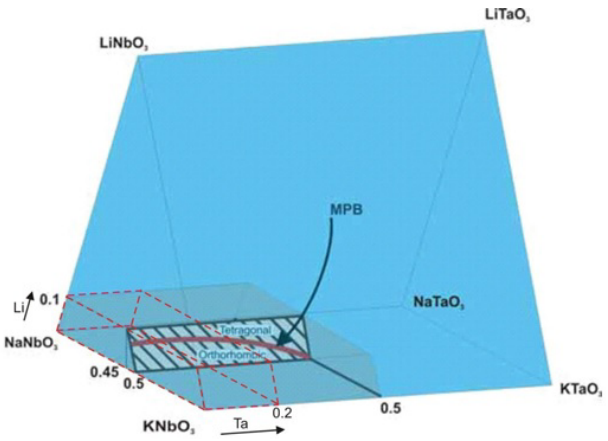

Fig. 1 Schematic representation of the phase space in the $(K_xNa_{1-x})_{1-y}Li_y(Nb_{1-z}Ta_z)O_3$ solid solution. The investigated phase space is shown with the red dotted line in the diagram.

Bragg angle. High temperature XRD measurements were carried out for selected compositions from room temperature to temperatures above their respective Curie temperatures. The diffraction patterns for some samples with very low potassium content were difficult to resolve into any particular phase. Synchrotron X-ray was therefore used to measure two of such samples from room temperature to temperatures above their cubic phases. Two of the diffraction patterns were refined using Rietveld refinement in Fullprof software [19]. Microstructural examination of the samples was done using a scanning electron microscope (SEM; LEO 1530, Gemini/Zeiss, Oberkochen, Germany). After polishing of the samples, they were chemically etched using Al_2O_3 based solution with the trade name MASTERMET. Silver paint was applied on both surfaces of the samples to act as electrode for the resistance and dielectric and piezoelectric property measurements. Unipolar strain hysteresis measurement was used to obtain the high signal piezoelectric charge coefficient values for the samples. The dielectric properties and resistance values were measured using a measuring robot attached to a precision LCR meter (HP 4284A, Palo Alto, CA, USA) and a digital high resistance meter (Agilent 4339B, Santa Clara, CA, USA), respectively. The resistivity values for the samples were calculated from the result of the resistance measurements. The strain hysteresis curves were obtained using an inductive transducer device (Hottinger Baldwin Messtechnik, Darmstadt, Germany). A complete hysteresis measurement was performed in 150 s.

3 Results and discussion

3. 1 Density

Figure 2 shows the relative density plot of $(K_xNa_{1-x})_{1-y}Li_y(Nb_{1-z}Ta_z)O_3$ (KNNLT) ceramics with 375 different compositions as a function of the amounts of the A- and B-site elements. The theoretical density was obtained by assuming both the intended compositions and the actual compositions are the same. The ratio between the amount of K^+ to that of Na^+ is varied with a 10 mol% increment interval. The Li^+ and Ta^{5+} contents of the samples are varied from 0 to 10 mol% and 0 to 20 mol%, respectively. The sintering temperatures used are dependent on the compositions of the samples. As the amount of Li^+ added increases, the sintering temperature used decreases, while increasing Ta^{5+} amount increases the sintering temperature required for optimum sintering. Due to the large number of samples involved, sintering was carried out in batches and this led to some samples well densified and others poorly densified. Samples with low density values (<92%) are due to sintering with either too high or too low sintering temperatures. For samples where the sintering was adequate, the average density value obtained is more than ~92%, and when compared with the results in the literature for similar compositions, they are 10%–20% less [13,20]. KNN compositions with no Li^+ or Ta^{5+} have density values ranged from 4.02 to 4.27 g/cm^3 (~89.1%–94.7%), and it is known that this value is difficult to exceed without pressure assisted sintering [2]. When only Li^+ is added to KNN, the density values increase with increasing amount of Li^+ added. This means that Li^+ improves densification without pressure assisted sintering, possibly due to its low melting temperature which forms a liquid phase during sintering thereby enabling particle rearrangement and better densification [21]. The effect of K^+ and Na^+ on density is such that at high concentration of each element, the density values are low, but as the amount of each element is similar, the density values are uniform. Ta^{5+} improves densification by pinning of the grain boundaries in the sample which leads to the formation of smaller grain sizes in KNN ceramics [22]. As the amount of Ta^{5+} added to the sample increases, the temperature required for effective sintering also increases probably due to its high melting point which means that higher temperatures are required to reach the activation energy necessary for sintering.

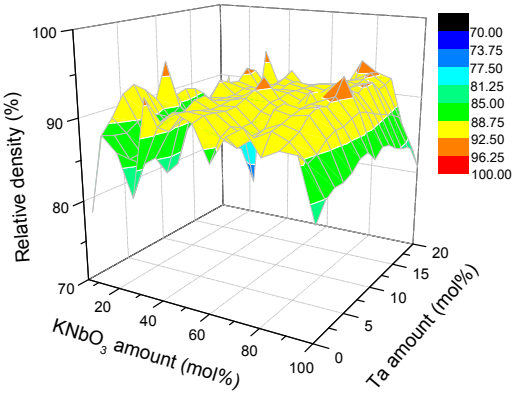

Fig. 2 Relative density values for $(K_xNa_{1-x})_{1-y}Li_y(Nb_{1-z}Ta_z)O_3$ solid solution where the K^+ content was varied from 10 to 100 mol%, while the Ta^{5+} content was varied from 0 to 20 mol%. Each measurement point on the graph represents an average of 5 data points. Depending on the composition of the samples, sintering temperatures ranging from 1050 to 1150 ℃ were used.

3. 2 Microstructure

The SEM images of the as-sintered and polished surfaces of selected samples are shown in Fig. 3. The grains in the as-sintered samples show a quasi-cubic morphology which is typical for KNN ceramics. Varying amounts of Li^+ and Ta^{5+} are used to show the effect of these elements on the average grain size. Increasing Li^+ addition leads to increasing grain growth, while the presence of Ta^{5+} tends to reduce the grain growth in the samples. This effect of Li^+ and Ta^{5+} in KNN ceramics has already been reported in the literature [23,24]. Although chemical segregation could not be observed with the high Ta doped $(K_xNa_{1-x})_{1-y}Li_yNbO_3$ (KLNN) compositions, there are reports in the literature where this phenomenon has been observed [25,26]. The presence of Li^+ in KNN ceramics increases the possibility that a liquid phase will be formed due to its low melting temperature. Ta^{5+} on the other hand has a high melting temperature which increases the activation energy required for sintering. It has been reported to inhibit fast movement of the grain boundaries during sintering, and as its amount increases, the sinter activity decreases [24]. Figure 3(a) shows the as-sintered microstructure for KNN ceramics modified with Li^+ and Ta^{5+}. Increasing the sintering temperature of the samples also results in increasing average grain size of the samples. Figure 3(b) shows KNN ceramics modified with 7 mol% each of Li^+ and Ta^{5+} and sintered at 1125 ℃. The grains have a bimodal grain size relationship with the large grains having an average size of (8.7±2.6) μm, while the

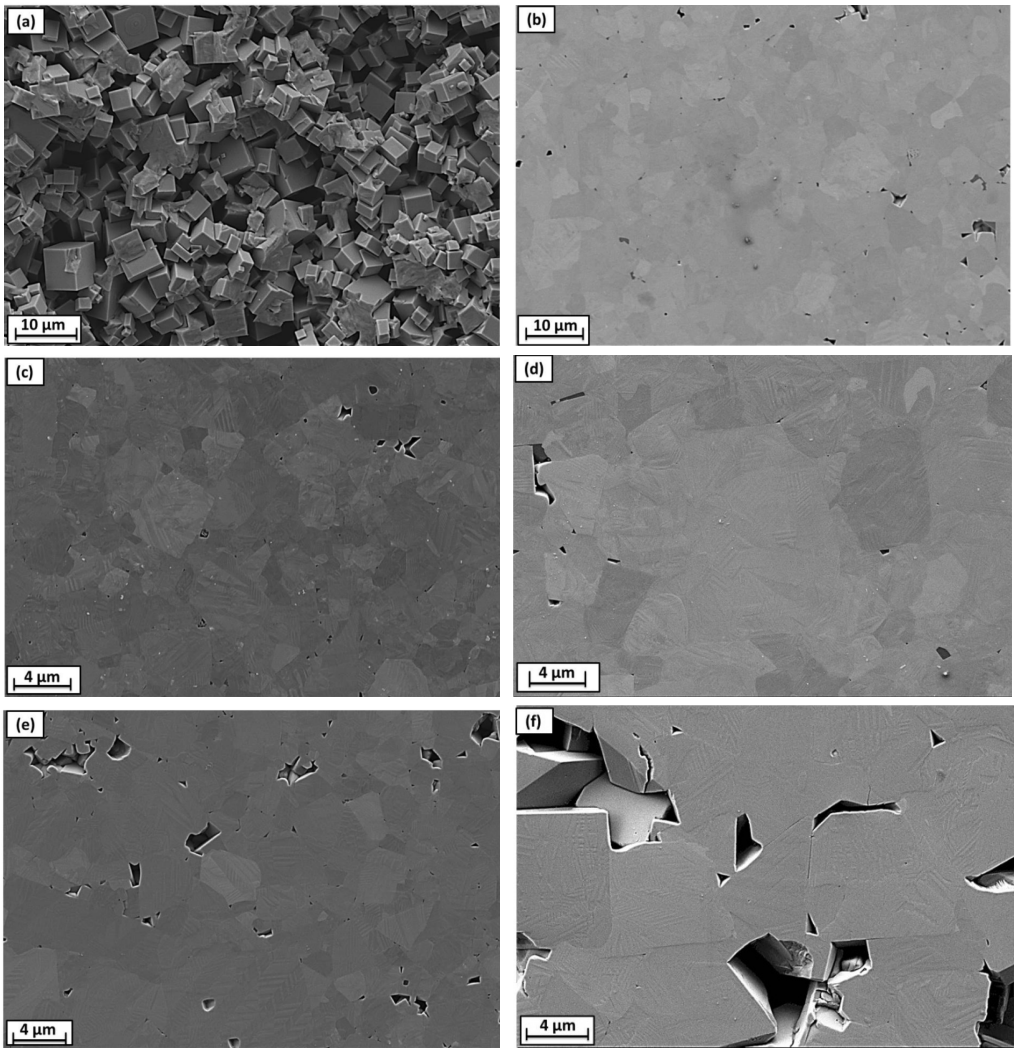

Fig. 3 SEM images of (a) as-sintered $(K_{0.475}Na_{0.475}Li_{0.05})(Nb_{0.95}Ta_{0.05})O_3$ ceramics sintered at 1125 ℃, (b) polished $(K_{0.465}Na_{0.465}Li_{0.07})(Nb_{0.93}Ta_{0.07})O_3$ ceramics sintered at 1125 ℃, (c) polished $(K_{0.48}Na_{0.48}Li_{0.04})(Nb_{0.96}Ta_{0.04})O_3$ ceramics sintered at 1075 ℃, (d) polished $(K_{0.4875}Na_{0.4875}Li_{0.025})(Nb_{0.95}Ta_{0.05})O_3$ ceramics sintered at 1125 ℃, (e) polished $(K_{0.495}Na_{0.495}Li_{0.01})(Nb_{0.99}Ta_{0.01})O_3$ ceramics sintered at 1075 ℃, and (f) polished $(K_{0.5}Na_{0.5})(Nb_{0.99}Ta_{0.01})O_3$ ceramics sintered at 1125 ℃.

average size for the small grains is (3.5±1.1) μm. Figure 3(c) shows polished $(K_{0.48}Na_{0.48}Li_{0.04})(Nb_{0.96}Ta_{0.04})O_3$ ceramics sintered at 1075 ℃ also with a bimodal grain size distribution where the larger grains have an average size of (3.2±0.8) μm, while the small grains have an average size of (1.4±0.8) μm. Figure 3(d) shows KNN ceramics with 2.5 mol% Li^+ and 5 mol% Ta^{5+} sintered at 1125 ℃. A unimodal grain size distribution is obtained with an average grain size of (2.8±1.5) μm. While Fig. 3(e) contained 1 mol% each of Li^+ and Ta^{5+} respectively and was sintered at 1075 ℃. The average grain size in Fig. 3(e) is (3.5±1.6) μm. Figure 3(f) shows KNN ceramics with 1 mol% Ta^{5+} sintered at 1125 ℃. A bimodal grain size distribution is also observed with the big grains having a size of (5.0±1.3) μm and the small grains having a size of (1.7±0.6) μm. Closer examination of the microstructures in Figs. 3(b)–3(f) indicates the presence of ferroelectric domains in the samples. This is an indication of ferroelectricity in the samples and also shows enhancement in the piezoelectric properties of KNN ceramics modified with Li^+ and Ta^{5+}.

3. 3 X-ray diffraction

Figure 4(a) shows representative diffraction patterns observed for all the samples. Orthorhombic phases, orthorhombic phases with an extra phase, two-phase boundaries (i.e., orthorhombic–tetragonal), two-phase boundaries with an extra phase, and tetragonal phases are observed in the patterns. The addition of high amounts of Li^+ and Ta^{5+} to KNN induces a phase transformation from an orthorhombic phase to a tetragonal phase. Between the two phases is a two-phase boundary which is a combination of both orthorhombic and tetragonal phases and has been reported [27,28]. This two-phase boundary was initially reported as an MPB just like in PZT [29], but further investigations show that the piezoelectric properties depend strongly on temperature and so the term "polymorphic phase boundary" is more appropriate. As the amount of Li^+ and Ta^{5+} in KNN increases, the phases begin to coexist at lower temperatures in the samples. Li^+ has a limited solid solubility in KNN and above 7 mol%, an extra phase related to the tungsten bronze structures $K_3Li_2Nb_5O_{15}$, $K_3LiNb_6O_{17}$ (00-036-0533), $K_3Li_2Nb_5O_{15}$ (00-023-1198), and $K_{0.73}Li_{0.27}TaO_3$ is formed [23,30].

Based on the diffraction patterns and the observed phases for all the samples, a phase map has been produced as shown in Fig. 4(b). When the amount of Ta is between 0 and 5 mol% for all $KNbO_3$ contents, the orthorhombic phase is the dominant phase. The phase diagram of KNN ceramics shows that at room temperature and $KNbO_3$ amounts between 10 and 30 mol%, the phase present is monoclinic but can sometimes be confused with the orthorhombic phase [29]. In order to simplify things, the orthorhombic phase has been used to represent this region. A greater portion of the phase space is represented using the two-phase coexistence between the orthorhombic and tetragonal phases. The tetragonal phase is represented by a small part of the phase space, i.e., Ta amount between 15 and 20 mol% and the $KNbO_3$ amount between 30 and 100 mol%. The presence of Ta in KNN ceramics tends to stabilize the tetragonal phase by decreasing the tetragonal–orthorhombic phase boundary to lower temperatures. The effect of $KNbO_3$ on KNN ceramics is to stabilize the orthorhombic phase provided the amount of Ta present is less than or equal to 5 mol%.

In some cases, the laboratory X-ray device recorded diffraction patterns which could not be assigned to any particular phase. Two examples of such samples are $(K_{0.09}Na_{0.81}Li_{0.1})(Nb_{0.95}Ta_{0.05})O_3$ and $(K_{0.185}Na_{0.74}Li_{0.075})(Nb_{0.95}Ta_{0.05})O_3$ compositions. It was not clear if they even have the perovskite phase. An opportunity arose where we could make measurements using synchrotron radiation for these two compositions. The results of the measurements are used to extract the lattice parameters for these compositions as shown in Figs. 4(c) and 4(d). It is clear that the two compositions crystallize in the perovskite structure and the sequence of phase transition from room temperature to temperatures above the Curie temperature (T_C) is orthorhombic to tetragonal and finally to the cubic phase. It is clear that as the amount of K^+ in the samples increases, transition region is lower, and more Li^+ amounts result in an increase in the Curie temperature.

High temperature XRD measurements have also been carried out on some selected samples from room temperature to ~600 ℃. The temperature steps used for the measurements are as follows. A 20 ℃ measurement interval from room temperature up to 220 ℃ and from 320 to 420 ℃ is used. A 10 ℃ measurement interval from 230 to 300 ℃ and from 430 to 550 ℃ is used. Finally a 50 ℃ step from 550 to 650 ℃ is used. Twelve $(K_xNa_{1-x})_{1-y}Li_y(Nb_{1-z}Ta_z)O_3$ samples with different compositions are measured and they are as follows:

$(K_{0.1}Na_{0.9})NbO_3$, $(K_{0.09}Na_{0.81}Li_{0.1})NbO_3$,

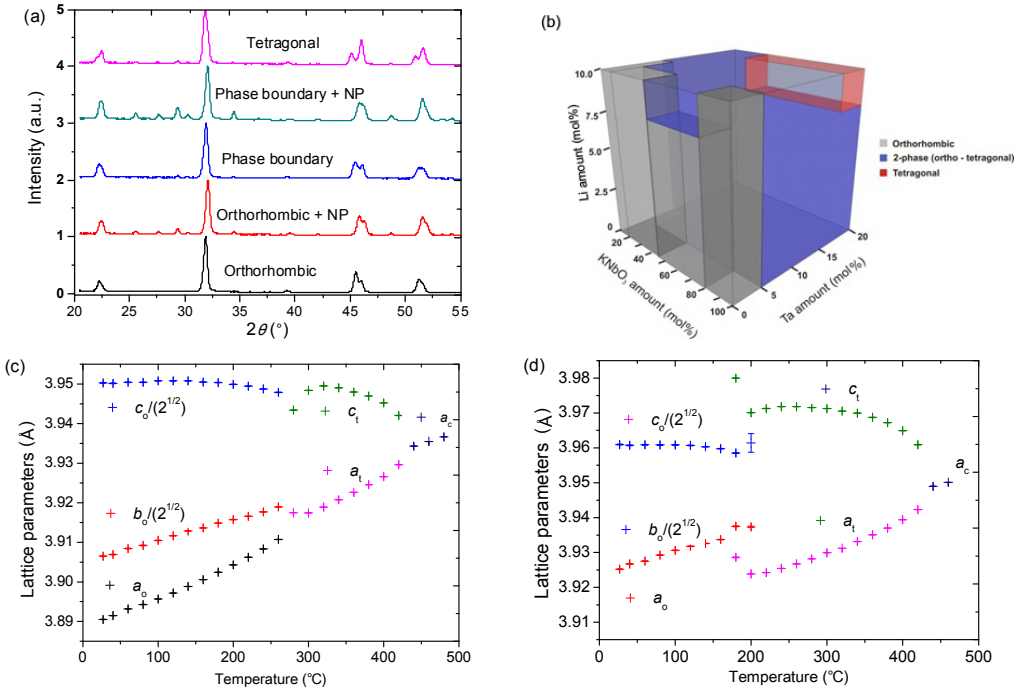

Fig. 4 (a) Characteristic XRD patterns showing the representation of the orthorhombic phase, the two-phase orthorhombic–tetragonal mixture, the tetragonal phase, and some non-perovskite (NP) phase. Extra phases which are identified as tungsten bronze phases could be observed in some patterns. (b) A plot of the phase space for the different phases observed in the $(K_xNa_{1-x})_{1-y}Li_y(Nb_{1-z}Ta_z)O_3$ ceramic library where {{x, 0.1, 1.0},{y, 0, 0.1},{z, 0, 0.2}}. The XRD measurements were carried out at room temperature on 6 different spots on the surface of the sample. Three major phases namely the orthorhombic phase, the tetragonal phase, and two-phase orthorhombic–tetragonal mixture in addition to second phases are observed. (c) and (d) Plots of the lattice parameters of $(K_{0.09}Na_{0.81}Li_{0.1})(Nb_{0.95}Ta_{0.05})O_3$ and $(K_{0.185}Na_{0.74}Li_{0.075})(Nb_{0.95}Ta_{0.05})O_3$ ceramics as a function of temperature, respectively. The legends a_o, b_o, and c_o represent the parameters for the orthorhombic phase, a_t and c_t represent the tetragonal phase, while a_c represents the cubic phase.

$(K_{0.285}Na_{0.665}Li_{0.05})(Nb_{0.85}Ta_{0.15})O_3$,
$(K_{0.2775}Na_{0.6475}Li_{0.075})(Nb_{0.85}Ta_{0.15})O_3$,
$(K_{0.45}Na_{0.45}Li_{0.1})(Nb_{0.9}Ta_{0.1})O_3$,
$(K_{0.57}Na_{0.38}Li_{0.05})(Nb_{0.9}Ta_{0.1})O_3$,
$(K_{0.6475}Na_{0.2775}Li_{0.075})(Nb_{0.85}Ta_{0.15})O_3$,
$(K_{0.63}Na_{0.27}Li_{0.1})(Nb_{0.8}Ta_{0.2})O_3$,
$(K_{0.78}Na_{0.195}Li_{0.025})(Nb_{0.8}Ta_{0.2})O_3$,
$(K_{0.855}Na_{0.095}Li_{0.05})(Nb_{0.8}Ta_{0.2})O_3$,
$(K_{0.81}Na_{0.09}Li_{0.1})(Nb_{0.8}Ta_{0.2})O_3$,
$(K_{0.9}Li_{0.1})NbO_3$.

Five different phases namely orthorhombic, tetragonal, two-phase orthorhombic–tetragonal, two-phase tetragonal–cubic, and cubic phase are observed. Some of the two-phase mixtures may actually be a single phase, but the resolution of the XRD is low so they could not be resolved. When there is little or no Ta present, the orthorhombic phase is observed, and with medium amounts of Li and Ta in the samples, these two-phase mixtures are observed. Ta amounts between 15 and 20 mol% favor the formation of the tetragonal phase and lowers the T_C values. A summary of the measured compositions, the phases involved, and the temperatures of phase transition are shown in Table 1.

3. 4 Dielectric properties

Figure 5(a) shows the dielectric constant values for $(K_xNa_{1-x})_{1-y}Li_y(Nb_{1-z}Ta_z)O_3$ solid solution measured at 1 kHz where the K^+ content was varied from 10 to 100 mol% while the Ta^{5+} content was varied from 0 to 20 mol%. The Li^+ content on the A-site was varied from 0 to 10 mol% but cannot be directly observed from the graph, but its addition to KNN increases the dielectric constant values. When the composition is close to or at the phase boundary, the dielectric constant values are higher than for compositions that are far from the phase boundary. The data points with sharp decrease in the values of the dielectric constant correspond to samples with low density values. As the amount of $KNbO_3$ increases, the dielectric constant values gradually increases. The effect of Ta on the values of the dielectric constant is less pronounced but increasing Ta amounts also increases the dielectric

Table 1 Compositions of the samples used for high temperature XRD measurements, the phases present in the samples, and the phase transition temperatures

Composition	Temperature (℃)				
	Orthorhombic	Tetragonal	Two-phase O–T	Two-phase T–C	Cubic
$(K_{0.1}Na_{0.9})NbO_3$	24–171	275–395	178–257	404–422	431
$(K_{0.09}Na_{0.81}Li_{0.1})NbO_3$	149–275	293–404	24–134		422
$(K_{0.285}Na_{0.665}Li_{0.05})(Nb_{0.85}Ta_{0.15})O_3$		134–379	24–120		387
$(K_{0.2775}Na_{0.6475}Li_{0.075})(Nb_{0.85}Ta_{0.15})O_3$		90–387	24–75	395–404	413
$(K_{0.45}Na_{0.45}Li_{0.1})(Nb_{0.9}Ta_{0.1})O_3$		120–309	24–105	327–395	404
$(K_{0.57}Na_{0.38}Li_{0.05})(Nb_{0.9}Ta_{0.1})O_3$		24–413			413
$(K_{0.6475}Na_{0.2775}Li_{0.075})(Nb_{0.85}Ta_{0.15})O_3$		68–336	24–53	345–395	404
$(K_{0.63}Na_{0.27}Li_{0.1})(Nb_{0.8}Ta_{0.2})O_3$		24–293		309–361	370
$(K_{0.78}Na_{0.195}Li_{0.025})(Nb_{0.8}Ta_{0.2})O_3$		75–257	24–68	275–327	336
$(K_{0.855}Na_{0.095}Li_{0.05})(Nb_{0.8}Ta_{0.2})O_3$		68–193	24–53	200–275	293
$(K_{0.81}Na_{0.09}Li_{0.1})(Nb_{0.8}Ta_{0.2})O_3$		24–293		309–345	352
$(K_{0.9}Li_{0.1})NbO_3$	24–208	240–482	215–223		565

constant values. Compared to results from the literature produced using the conventional mixed-oxide synthesis method, the obtained dielectric constant values are 10%–20% lower [13,18,25,31,32].

Relatively high dielectric loss values are obtained for the KNNLT samples measured at 1 kHz (Fig. 5(b)). Most of the compositions with high dielectric loss values correspond to samples with either very low density or extra phases. In most cases also, KNN

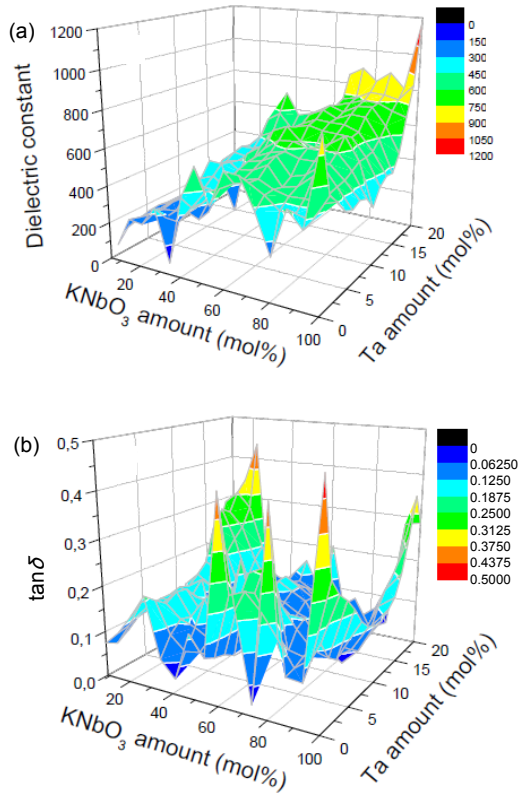

Fig. 5 Graphs showing (a) the dielectric constant values for $(K_xNa_{1-x})_{1-y}Li_y(Nb_{1-z}Ta_z)O_3$ solid solution system as a function of the amounts of the A- and B-site elements at room temperature and (b) the dielectric loss values for the same samples at room temperature.

samples with relatively high dielectric constant values also tend to exhibit high loss values. This behavior is known to exist for $(Bi_{0.5}Na_{0.5})TiO_3$-based ceramics [33,34]. Compared to values in the literature for similar compositions, the loss values are about one order of magnitude higher [20,31,32,35]. The difference in the loss values could be attributed to the synthesis method and special atmospheres under which they were sintered. Oxygen atmosphere is known to give better resistivity to the samples than sintering in air atmosphere.

There is no direct correlation between the presence of a phase boundary and the dielectric loss values unlike with dielectric constant [13]. While some of the compositions at or close to the phase boundary show high loss values, others do not. In general, the dielectric loss values at or close to the phase boundary are uniform when compared to those compositions far away from them. Li^+ addition in KNN increases the dielectric loss because of its small ionic radius, while Ta^{5+} has been reported to decrease the value of the dielectric loss due to hindrance to the movement of the atoms in the ceramic [13].

3.5 Effect of density on the dielectric constant

In order to understand the effect of density on the dielectric constant, an analysis has been carried out where the dielectric constant is divided by the density as shown in Fig. 6. The plot shows that the influence of density on the dielectric constant is not very significant since the plot is similar to the dielectric constant graph. When the difference in density values is high, the effect on the dielectric constant becomes very significant. This behavior is different from PZT based ceramics where the decreasing density of the sample has a significant effect on the dielectric constant [36].

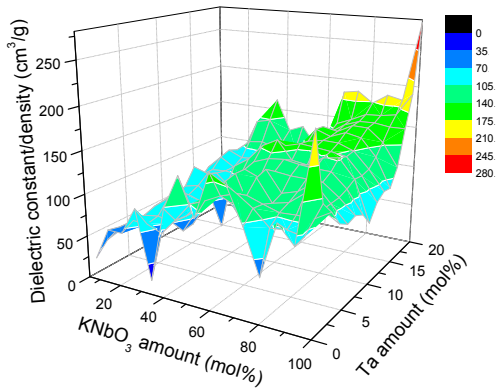

Fig. 6 A plot of the quotient between the dielectric constant and bulk density of the $(K_xNa_{1-x})_{1-y}Li_y(Nb_{1-z}Ta_z)O_3$ ceramics as a function of the amounts of $KNbO_3$ and Ta.

3. 6 Resistivity

Figure 7 shows the resistivity graph for $(K_xNa_{1-x})_{1-y}Li_y(Nb_{1-z}Ta_z)O_3$ solid solution system as a function of the amounts of $KNbO_3$ and Ta. The colour scale gives an indication of the obtained logarithm of the resistivity values for the samples. The black colour is for samples whose resistivity values could not be measured due to cracks and other defects. The obtained results vary from batch to batch in the samples. Low values are obtained for samples with K^+ content of 50 mol% compared to the others. This could be because more second phases are observed here. Resistivity values for samples close to or at the phase boundary are generally not higher than those at other regions. Resistivity values obtained range from 10^9 to 10^{13} Ω·cm. Ta increases the resistivity of KNN [13], but its effect on the samples in this measurement is minimal. There is a very strong effect of the density of the samples on the resistivity. Samples with low density values have low resistivity values and vice versa.

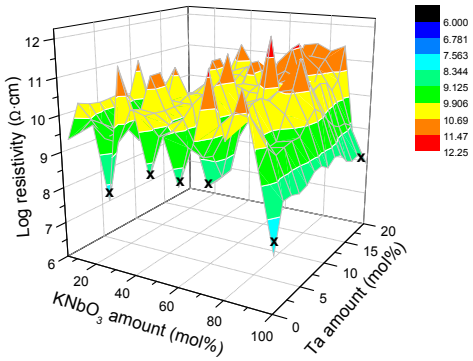

Fig. 7 A plot of the resistivity in logarithm form for $(K_xNa_{1-x})_{1-y}Li_y(Nb_{1-z}Ta_z)O_3$ solid solution as a function of the amounts of $KNbO_3$ and Ta. The areas marked X represent the samples that were either cracked or had poor sintering behavior.

3. 7 Piezoelectric charge coefficient (d_{33}^*)

The large signal piezoelectric charge coefficient values for compositions where K^+ amounts are ~60 mol% is shown in Fig. 8(a). A phase boundary exists in this phase space between the orthorhombic and the tetragonal phases. The d_{33}^* values are measured for the compositions close to the phase boundary and those far from it. The plot (Fig. 8(a)) shows that the highest d_{33}^* values are obtained for compositions close to this boundary. Figure 8(b) shows the result of d_{33}^* values for all compositions. Most of the compositions when K^+ amount ranges from 0 to 50 mol% show very low piezoelectric activity possibly because of low density values and the presence of extra phases in the patterns. Increasing amounts of K^+ and Ta^{5+} in the samples increases the d_{33}^* values. Compared to the results from similar compositions in the literature, the obtained values for the good samples are 10%–20% less and more than 30% for the less dense samples [13,18,20,31,37].

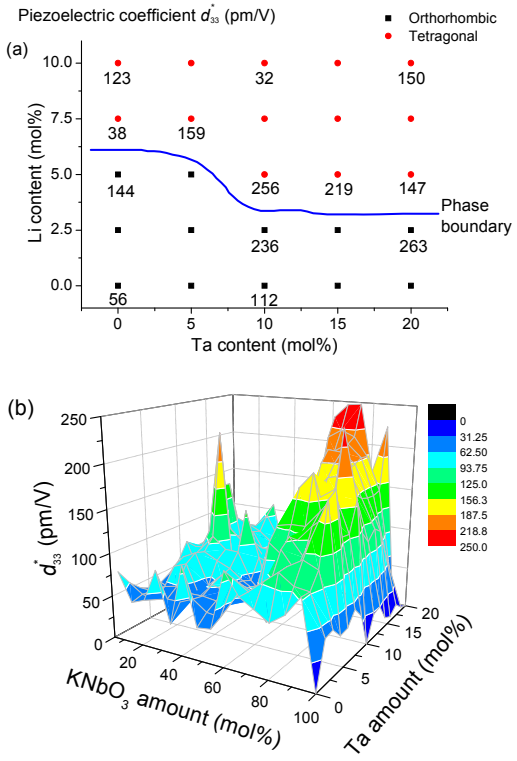

Fig. 8 (a) Large signal piezoelectric charge coefficient values for selected compositions in the $(K_xNa_{1-x})_{1-y}Li_y(Nb_{1-z}Ta_z)O_3$ solid solution system with K^+ content of 60 mol%, where Li^+ content varies from 0 to 10 mol% and Ta^{5+} content from 0 to 20 mol%; (b) d_{33}^* values for all the samples as a function of $KNbO_3$ and Ta amounts.

4 Conclusions

A library of ceramic compounds based on the $(K_xNa_{1-x})_{1-y}Li_y(Nb_{1-z}Ta_z)O_3$ solid solution have been produced using high-throughput experimentation (HTE) method. Apparent density values of ~92% are obtained for samples which are very well sintered while the density is less for poorly sintered samples. The diffraction patterns show that new phase boundaries between an orthorhombic phase and a tetragonal phase are observed as the amounts of Li^+ and Ta^{5+} in KNN ceramics increases. The dielectric constant values show that increasing $KNbO_3$ and Ta amounts leads to increasing dielectric constant values. Low density values seem to have very little influence on the dielectric constant values. The dielectric loss values are also high and are attributed mainly to the low density values. The resistivity values range from ~10^9 to 10^{13} Ω·cm and the density has a clear influence on the resistivity. The piezoelectric properties at the phase boundaries are higher than for compositions far from the boundary. These new phase boundaries however do not translate into much higher piezoelectric charge coefficient values as expected. The high-throughput method is a very fast way to screen samples but it is not appropriate to obtain the correct properties of the samples. Compared to the conventional method, all the properties of the samples measured are lower.

Acknowledgements

The research leading to these results has received financial support from the Deutsche Forschungs Gemeinschaft (DFG) under Grant No. SCHN 372/16:1-2.

References

[1] European Parliament and Council. Directive 2002/95/EC of the European parliament and of the council of January 2003 on the restriction of the use of hazardous substances in electrical and electronic equipment. *European Journal* 2003, **37**: 1–9.

[2] Egerton L, Dillon DM. Piezoelectric and dielectric properties of ceramics in the system potassium—Sodium niobate. *J Am Ceram Soc* 1959, **42**: 438–442.

[3] Li J-F, Wang K, Zhu F-Y, *et al*. (K,Na)NbO_3-based lead-free piezoceramics: Fundamental aspects, processing technologies, and remaining challenges. *J Am Ceram Soc* 2013, **96**: 3677–3696.

[4] Wang K, Li J-F. (K,Na)NbO_3-based lead-free piezoceramics: Phase transition, sintering and property enhancement. *J Adv Ceram* 2012, **1**: 24–37.

[5] Smolenskii GA, Isupov VA, Agranovskaya AI, *et al*. New ferroelectrics of complex composition. *Sov Phys Solid State (Engl Transl)* 1961, **2**: 2651–2654.

[6] Takenaka T, Maruyama K-i, Sakata K. $(Bi_{1/2}Na_{1/2})TiO_3$–$BaTiO_3$ system for lead-free piezoelectric ceramics. *Jpn J Appl Phys* 1991, **30**: 2236.

[7] Cawse JN. Experimental strategies for combinatorial and high-throughput materials development. *Acc Chem Res* 2001, **34**: 213–221.

[8] Schmatloch S, Schubert US. Techniques and instrumentation for combinatorial and high-throughput polymer research: Recent developments. *Macromol Rapid Comm* 2004, **25**: 69–76.

[9] Chang H, Gao C, Takeuchi I, *et al*. Combinatorial synthesis and high throughput evaluation of ferroelectric/dielectric thin-film libraries for microwave applications. *Appl Phys Lett* 1998, **72**: 2185.

[10] Chang H, Takeuchi I, Xiang XD. A low-loss composition region identified from a thin-film composition spread of $(Ba_{1-x-y}Sr_xCa_y)TiO_3$. *Appl Phys Lett* 1999, **74**: 1165.

[11] Stegk TA, Janssen R, Schneider GA. High-throughput synthesis and characterization of bulk ceramics from dry powders. *J Comb Chem* 2008, **10**: 274–279.

[12] Stegk TA, Mgbemere H, Herber R-P, *et al*. Investigation of phase boundaries in the system $(K_xNa_{1-x})_{1-y}Li_y(Nb_{1-z}Ta_z)O_3$ using high-throughput experimentation (HTE). *J Eur Ceram Soc* 2009, **29**: 1721–1727.

[13] Saito Y, Takao H. High performance lead-free piezoelectric ceramics in the (K,Na)NbO_3–$LiTaO_3$ solid solution system. *Ferroelectrics* 2006, **338**: 17–32.

[14] Shrout TR, Zhang SJ. Lead-free piezoelectric ceramics: Alternatives for PZT? *J Electroceram* 2007, **19**: 113–126.

[15] Skidmore TA, Milne SJ. Phase development during mixed-oxide processing of a $[Na_{0.5}K_{0.5}NbO_3]_{1-x}$–$[LiTaO_3]_x$ powder. *J Mater Res* 2007, **22**: 2265–2272.

[16] Kim M-S, Lee D-S, Park E-C, *et al*. Effect of Na_2O additions on the sinterability and piezoelectric properties of lead-free $95(Na_{0.5}K_{0.5})NbO_3$–$5LiTaO_3$ ceramics. *J Eur Ceram Soc* 2007, **27**: 4121–4124.

[17] Kim M-S, Jeong S-J, Song J-S. Microstructures and piezoelectric properties in the Li_2O-excess $0.95(Na_{0.5}K_{0.5})NbO_3$–$0.05LiTaO_3$ ceramics. *J Am Ceram Soc* 2007, **90**: 3338–3340.

[18] Chang Y, Yang Z, Ma D, *et al*. Phase coexistence and high electrical properties in $(K_xNa_{0.96-x}Li_{0.04})(Nb_{0.85}Ta_{0.15})O_3$ piezoelectric ceramics. *J Appl Phys* 2009, **105**: 054101.

[19] Rodríguez-Carvajal J. Recent advances in magnetic structure determination by neutron powder diffraction. *Physica B* 1993, **192**: 55–69.

[20] Hollenstein E, Davis M, Damjanovic D, *et al*. Piezoelectric properties of Li- and Ta-modified $(K_{0.5}Na_{0.5})NbO_3$ ceramics. *Appl Phys Lett* 2005, **87**: 182905.

[21] Matsubara M, Yamaguchi T, Kikuta K, *et al*. Effect of Li substitution on the piezoelectric properties of potassium sodium niobate ceramics. *Jpn J Appl Phys* 2005, **44**: 6136.

[22] Matsubara M, Yamaguchi T, Kikuta K, *et al*. Synthesis and characterization of $(K_{0.5}Na_{0.5})(Nb_{0.7}Ta_{0.3})O_3$ piezoelectric ceramics sintered with sintering aid $K_{5.4}Cu_{1.3}Ta_{10}O_{29}$. *Jpn J Appl Phys* 2005, **44**: 6618.

[23] Klein N, Hollenstein E, Damjanovic D, *et al*. A study of the phase diagram of $(K,Na,Li)NbO_3$ determined by dielectric and piezoelectric measurements, and Raman spectroscopy. *J Appl Phys* 2007, **102**: 014112.

[24] Matsubara M, Kikuta K, Hirano S. Piezoelectric properties of $(K_{0.5}Na_{0.5})(Nb_{1-x}Ta_x)O_3$−$K_{5.4}CuTa_{10}O_{29}$ ceramics. *J Appl Phys* 2005, **97**: 114105.

[25] Wang Y, Damjanovic D, Klein N, *et al*. Compositional inhomogeneity in Li- and Ta-modified $(K,Na)NbO_3$ ceramics. *J Am Ceram Soc* 2007, **90**: 3485–3489.

[26] Zhen Y, Li J-F. Abnormal grain growth and new core–shell structure in $(K,Na)NbO_3$-based lead-free piezoelectric ceramics. *J Am Ceram Soc* 2007, **90**: 3496–3502.

[27] Mgbemere HE, Hinterstein M, Schneider GA. Electrical and structural characterization of $(K_xNa_{1-x})NbO_3$ ceramics modified with Li and Ta. *J Appl Cryst* 2011, **44**: 1080–1089.

[28] Mgbemere HE, Fernandes RP, Hinterstein M, *et al*. Temperature-dependent synchrotron powder diffraction phase studies of $(K_{0.37}Na_{0.52}Li_{0.03})(Nb_{0.87}Ta_{0.1}Sb_{0.03})O_3$ ferroelectric ceramics**.** *Zeitschrift für Kristallographie Crystalline Materials* 2011, **226**: 138–144.

[29] Jaffe B, Jaffe H, Cook WR. *Piezoelectric Ceramics*. London: Academic Press, 1971.

[30] Guo Y, Kakimoto K-i, Ohsato H. Phase transitional behavior and piezoelectric properties of $(Na_{0.5}K_{0.5})NbO_3$–$LiNbO_3$ ceramics. *Appl Phys Lett* 2004, **85**: 4121.

[31] Wu L, Zhang J, Zheng P, *et al*. Influences of morphotropic phase boundaries on physical properties in $(K,Na,Li)Nb_{0.80}Ta_{0.20}O_3$ ceramics. *J Phys D: Appl Phys* 2007, **40**: 3527.

[32] Zuo R, Röedel J, Chen R, *et al*. Sintering and electrical properties of lead-free $Na_{0.5}K_{0.5}NbO_3$ piezoelectric ceramics. *J Am Ceram Soc* 2006, **89**: 2010–2015.

[33] Herabut A, Safari A. Processing and electromechanical properties of $(Bi_{0.5}Na_{0.5})_{(1-1.5x)}La_xTiO_3$ ceramics. *J Am Ceram Soc* 1997, **80**: 2954–2958.

[34] Wu L, Xiao D-Q, Lin D-M, *et al*. Synthesis and properties of $[Bi_{0.5}(Na_{1-x}Ag_x)_{0.5}]_{1-y}Ba_yTiO_3$ piezoelectric ceramics. *Jpn J Appl Phys* 2005, **44**: 8515.

[35] Ringgaard E, Wurlitzer T. Lead-free piezoceramics based on alkali niobates. *J Eur Ceram Soc* 2005, **25**: 2701–2706.

[36] Dunn ML, Taya M. Electromechanical properties of porous piezoelectric ceramics. *J Am Ceram Soc* 1993, **76**: 1697–1706.

[37] Zhao P, Zhang B-P, Li J-F. Influences of sintering temperature on piezoelectric, dielectric and ferroelectric properties of Li/Ta-codoped lead-free $(Na,K)NbO_3$ ceramics. *J Am Ceram Soc* 2008, **91**: 1690–1692.